Computers and Concrete, Vol. 6, No. 6 (2009) 505-521
DOI: http://dx.doi.org/10.12989/cac.2009.6.6.505

Closed form ultimate strength of multi-rectangle reinforced concrete sections under axial load and biaxial bending

V. Dias da Silva†, M. H. F. M. Barros, E. N. B. S. Júlio and C. C. Ferreira

Department of Civil Engineering, University of Coimbra, Polo II-Pinhal de Marrocos, 3030-290 Coimbra,, Portugal

(Received March 22, 2006, Accepted November 24, 2009)

Abstract. The analysis of prismatic members made of reinforced concrete under inclined bending, especially the computation of ultimate loads, is a pronounced non-linear problem which is frequently solved by discretizing the stress distribution in the cross-section using interpolation functions. In the approach described in the present contribution the exact analytical stress distribution is used instead. The obtained expressions are integrated by means of a symbolic manipulation package and automatically converted to optimized Fortran code. The direct problem-computation of ultimate internal forces given the position of the neutral axis-is first described. Subsequently, two kinds of inverse problem are treated: the computation of rupture envelops and the dimensioning of reinforcement, given design internal forces. An iterative Newton-Raphson procedure is used. Examples are presented.

Keywords: reinforced concrete sections; ultimate limit state; prismatic members; inclined bending; formulation; design.

1. Introduction

The computation of the behaviour of reinforced concrete prismatic members under bending is a pronounced non-linear problem, especially in loading cases in which the material is close to rupture, since in these cases its rheological behaviour cannot be represented with sufficient accuracy by a linear law.

This problem is frequently solved by numerical means, where the stress distribution in the cross-section is approximated using interpolation functions. Fafitis (2001) presented a method for the computation of the stresses in reinforced concrete sections using Green's Theorem. It is based on the transformation of the double integrals in the equilibrium equations into line integrals along the perimeter of the compressed concrete section. Gauss-Legendre quadrature is then used in the line integration. If the stress-strain relation for concrete is defined by polynomials up to the third degree the three point integration scheme yields the exact result. For this reason the method is exact if the stress-strain law of concrete is described by the parabola-rectangle law. If other complex constitutive equations as the ones indicated in Eurocode (2004) and Model Code (1990), are used the method gives approximate results. Bonet *et al.* (2004) presented two methods based on Gauss quadrature

† Associate Professor, Corresponding author, E-mail: vdsilva@dec.uc.pt

and division of the compression zone into layers. Brondum (1987) and Yen (1991) performed these integrations but using constant stress diagram. Rodrigues *et al.* (1999) proposed the resolution by decomposing the section into trapezes. Other methods are based on the definition of a fiber mesh of the total cross-section including the reinforcement bars. The number of them depends on the desired accuracy. These methods are used by Sfakianakis (2002). Charalampakisa *et al.* (2008) present also a work with a fiber algorithm where the cross section is described by multi-nested curvilinear polygons.

In a work from De Vivo and Rosati (1998) the equilibrium nonlinear equations of the section, submitted to axial load and bending moment, are solved by two algorithms. These are based on a secant strategy where the nonlinear constitutive law of concrete is replaced by a linear one of secant type. The method is improved with a tangent approach in Alfano *et al.* (2007). Other algorithms are presented by Rosati *et al.* (2008) with different schemes to evaluate ultimate axial load and bending moments of the reinforced concrete sections. Another work from Zupan and Saje (2006) considers an analytical integration of stress field over concrete cross sections with a uniaxial stress-strain relation for concrete given by a smooth simplified function.

Barros *et al.* (2004) proposed the use of Heaviside functions for the definition of the stress-strain law and the rupture conditions and performing the exact integration by the use of mathematical manipulation programs. Lately in Barros *et al.* (2005) the method is applied to the evaluation of interaction surfaces of rupture in biaxial bending, with application to complex sections. This method is used in the present work. The integration of the stresses in the cross-section is performed analytically, so that no interpolation functions are needed. Thus, the computation of the internal forces which correspond to a given deformation is exact. In the case of the inverse problem–computation of the deformations for given internal forces–although the problem is solved by numerical means–the Newton-Raphson algorithm is used–the solution may also be considered as exact, since no interpolations are used and the iterative procedure is stopped only when the error attains a negligible value.

2. Computation of internal forces

The internal forces are computed as described by Barros *et al.* (2004, 2005), using expressions obtained by analytical integration of the one-dimensional stress-strain relations for compressed concrete and for steel. The integrations are performed by means of a symbolic manipulation program (Maple).

As the cross section is assumed to remain plain, three deformation parameters must be given. In this contribution these parameters are: the strain in the most compressed concrete fibre and two parameters defining the position of the neutral axis.

2.1. Constitutive equations

In what concerns the concrete, two constitutive laws are considered: the stress-strain relation defined by CEB-FIP (1991) (Fig. 1) and the equation defined in the Eurocode 2 (2004) (Fig. 2). For the steel an elastic perfectly plastic material law is considered, as represented in Fig. 3. Since the unloading behaviour of the reinforced concrete members is not analysed, there is no need to identify the elastic and plastic parts of the deformation.

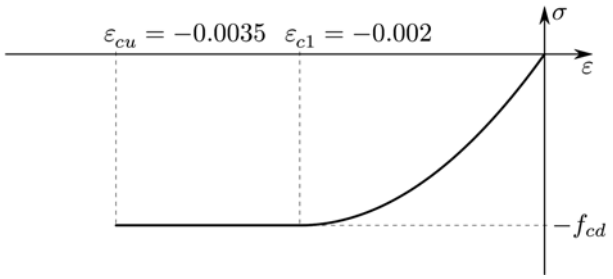

Fig. 1 Parabola-rectangle stress-strain relation for the concrete (CEB-FIP (1991))

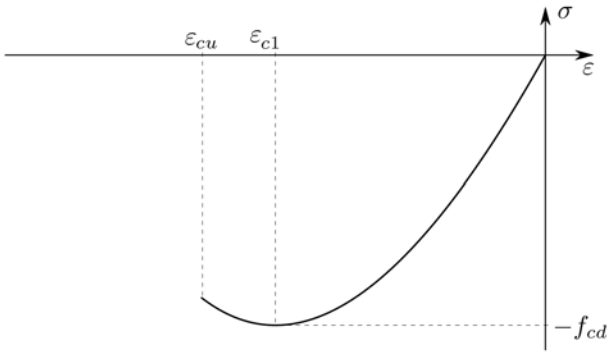

Fig. 2 Stress-strain relation defined in Eurocode 2 (2004)

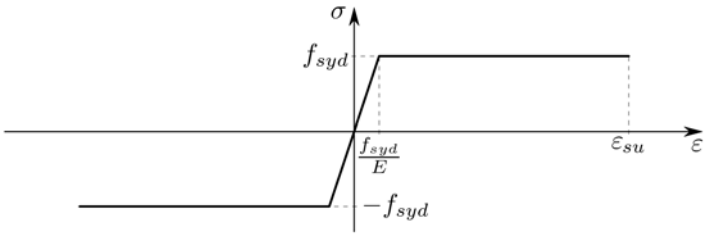

Fig. 3 Elastic perfectly plastic material law assumed for the reinforcing steel

The constitutive equations are described by single expressions, rather than parametric ones, which facilitates their analytical treatment by means of a symbolic manipulation package (Maple). The corresponding expressions for the concrete are

$$\sigma_c = \frac{f_{cd}}{\varepsilon_{c1}}\left(2\varepsilon + \frac{\varepsilon^2}{\varepsilon_{c1}}\right)H[\varepsilon + \varepsilon_{c1}] - f_{cd}H[-\varepsilon - \varepsilon_{c1}] \tag{1}$$

for the parabola-rectangle relation for the concrete, where H represents the Heaviside function, and

$$\sigma_c = \frac{\frac{E_{cc1\varepsilon}}{\varepsilon_{c1}} + \frac{\varepsilon^2}{\varepsilon_{c1}^2}}{1 - (E_{cc1} - 2)\frac{\varepsilon}{\varepsilon_{c1}}} f_{cd} \tag{2}$$

for the constitutive law defined in (European 2004). The main difference between these two laws

resides in the value of the ultimate strain, which is fixed in the CEB curve and variable with the class of concrete in the Eurocode curve.

Using the Heaviside function, the stress-strain relation for the steel (Fig. 3) may also be represented by a single expression, yielding

$$\sigma = f_{syd} H\left(\varepsilon - \frac{f_{syd}}{E}\right) + E\varepsilon H\left(\varepsilon + \frac{f_{syd}}{E}\right) - E\varepsilon H\left(\varepsilon - \frac{f_{syd}}{E}\right) - f_{syd} H\left(-\varepsilon - \frac{f_{syd}}{E}\right) \tag{3}$$

2.2. Computation of the internal forces

This section briefly describes the way as the concrete stress resultants are computed. The geometrical properties of the cross section are depicted in Fig. 4. The steel area is assumed to be distributed along the sides of a rectangle with the dimensions $(b\text{-}2a)\times(h\text{-}2a)$. The amount of steel may then be defined by the thickness of each side (a_1, a_2, a_3 and a_4).

For the computation of the contribution of the concrete stresses to the internal forces, five cases must be considered, as represented in Fig. 5. Angle β may take values in the interval $0<\beta<\frac{\pi}{2}$. Other alternatives correspond to changes of the reference corner, which coincides with the most compressed concrete fibre.

The formal expressions for the computation of the stress resultants in terms of the reference axes depicted in Fig. 4 are, for the five cases (Fig. 5)

Case I: $\begin{cases} X \le b \sin \beta \\ X \le h \cos \beta \end{cases}$

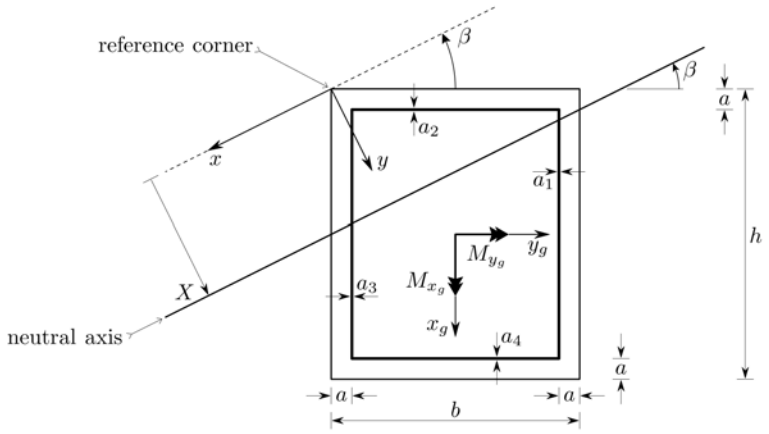

Fig. 4 Geometrical properties and reference axes for the concrete stresses

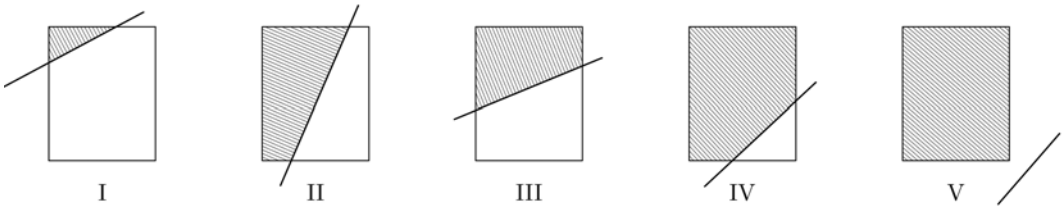

Fig. 5 The five alternatives considered in the computation of the concrete stress resultants

$$N_c = \frac{1}{\sin\beta\cos\beta}\int_0^X \sigma_c y dy$$
$$M_{cx} = \frac{1}{\sin\beta\cos\beta}\int_0^X \sigma_c y^2 dy \tag{4}$$
$$M_{cy} = \frac{1}{2}\frac{\cos^2\beta-\sin^2\beta}{\sin^2\beta\cos^2\beta}\int_0^X \sigma_c y^2 dy$$

Case II: $h\cos\beta < X \le b\sin\beta$

$$N_c = \frac{1}{\sin\beta\cos\beta}\int_0^{h\cos\beta} \sigma_c y dy + \frac{h}{\sin\beta}\int_{h\cos\beta}^X \sigma_c dy$$
$$M_{cx} = \frac{1}{\sin\beta\cos\beta}\int_0^{h\cos\beta} \sigma_c y^2 dy + \frac{h}{\sin\beta}\int_{h\cos\beta}^X \sigma_c y dy \tag{5}$$
$$M_{cy} = \frac{1}{2}\frac{\cos^2\beta-\sin^2\beta}{\sin^2\beta\cos^2\beta}\int_0^{h\cos\beta} \sigma_c y^2 dy + \int_{h\cos\beta}^X \left(\frac{h\cos\beta}{\sin^2\beta}y - \frac{h^2}{2\sin^2\beta}\right)\sigma_c dy$$

Case III: $b\sin\beta < X \le h\cos\beta$

$$N_c = \frac{1}{\sin\beta\cos\beta}\int_0^{b\sin\beta} \sigma_c y dy + \frac{b}{\cos\beta}\int_{b\sin\beta}^X \sigma_c dy$$
$$M_{cx} = \frac{1}{\sin\beta\cos\beta}\int_0^{b\sin\beta} \sigma_c y^2 dy + \frac{b}{\cos\beta}\int_{b\sin\beta}^X \sigma_c y dy \tag{6}$$
$$M_{cy} = \frac{1}{2}\frac{\cos^2\beta-\sin^2\beta}{\sin^2\beta\cos^2\beta}\int_0^{b\sin\beta} \sigma_c y^2 dy + \int_{b\sin\beta}^X \left(\frac{b^2}{2\cos^2\beta} - \frac{b\sin\beta}{\cos^2\beta}y\right)\sigma_c dy$$

Case IV: $\begin{cases} X > b\sin\beta \\ X > h\cos\beta \\ X \le b\sin\beta + h\cos\beta \end{cases}$

$$N_c = \frac{1}{\sin\beta\cos\beta}\int_0^{h\cos\beta} \sigma_c y dy + \frac{h}{\sin\beta}\int_{h\cos\beta}^X \sigma_c dy - \int_{b\sin\beta}^X \frac{y-b\sin\beta}{\sin\beta\cos\beta}\sigma_c dy$$
$$M_{cx} = \frac{1}{\sin\beta\cos\beta}\int_0^{h\cos\beta} \sigma_c y^2 dy + \frac{h}{\sin\beta}\int_{h\cos\beta}^X \sigma_c y dy - \int_{b\sin\beta}^X \frac{y-b\sin\beta}{\sin\beta\cos\beta}\sigma_c y dy$$
$$M_{cy} = \frac{1}{2}\frac{\cos^2\beta-\sin^2\beta}{\sin^2\beta\cos^2\beta}\int_0^{h\cos\beta} \sigma_c y^2 dy + \int_{h\cos\beta}^X \left(\frac{h\cos\beta}{\sin^2\beta}y - \frac{h^2}{2\sin^2\beta}\right)\sigma_c dy \tag{7}$$
$$- \int_{b\cos\beta}^X \frac{1}{2}\sigma_c\left[\frac{y^2(\cos^2\beta-\sin^2\beta)}{\sin^2\beta\cos^2\beta} - \frac{b^2}{\cos^2\beta} + \frac{2by\sin\beta}{\cos^2\beta}\right]dy$$

Case V: $X > b\sin\beta + h\cos\beta$

$$
\begin{aligned}
N_c &= \frac{1}{\sin\beta\cos\beta}\int_0^{h\cos\beta}\sigma_c y\,dy + \frac{h}{\sin\beta}\int_{h\cos\beta}^{b\sin\beta+h\cos\beta}\sigma_c\,dy - \int_{b\sin\beta}^{b\sin\beta+h\cos\beta}\frac{y-b\sin\beta}{\sin\beta\cos\beta}\sigma_c\,dy \\
M_{cx} &= \frac{1}{\sin\beta\cos\beta}\int_0^{h\cos\beta}\sigma_c y^2\,dy + \frac{h}{\sin\beta}\int_{h\cos\beta}^{b\sin\beta+h\cos\beta}\sigma_c y\,dy - \int_{b\sin\beta}^{b\sin\beta+h\cos\beta}\frac{y-b\sin\beta}{\sin\beta\cos\beta}\sigma_c y\,dy \\
M_{cy} &= \frac{1}{2}\frac{\cos^2\beta-\sin^2\beta}{\sin^2\beta\cos^2\beta}\int_0^{h\cos\beta}\sigma_c y^2\,dy + \int_{h\cos\beta}^{b\sin\beta+h\cos\beta}\left(\frac{h\cos\beta}{\sin^2\beta}y - \frac{h^2}{2\sin^2\beta}\right)\sigma_c\,dy \\
&\quad - \int_{b\sin\beta}^{b\sin\beta+h\cos\beta}\frac{1}{2}\sigma_c\left[\frac{y^2(\cos^2\beta-\sin^2\beta)}{\sin^2\beta\cos^2\beta} - \frac{b^2}{\cos^2\beta} + \frac{2by\sin\beta}{\cos^2\beta}\right]dy
\end{aligned}
\tag{8}
$$

The integrals contained in expressions (4) to (8) are analytically evaluated by using a symbolic manipulation package (Maple), after substitution of σ_c by expressions (1) or (2). The strain in the concrete, as a function of y (Fig. 4), is referred to the strain in the reference corner (most compressed concrete fibre) ε_c

$$\varepsilon = \varepsilon_c - \varepsilon_c\frac{y}{X} \tag{9}$$

The results are subsequently converted to optimized Fortran code.

If the ultimate internal forces of the cross section are to be computed, ε_c is given by

$$
\begin{cases} \varepsilon_c = -\dfrac{\alpha}{1-\alpha}\varepsilon_{su} & \text{if} \quad \alpha < \alpha_0 \\ \varepsilon_c = -\varepsilon_{cu} & \text{if} \quad \alpha \geq \alpha_0 \end{cases}
\quad \text{with} \quad
\begin{cases} \alpha = \dfrac{X}{d} \\ \alpha_0 = \dfrac{\varepsilon_{cu}}{\varepsilon_{cu}+\varepsilon_{su}} \end{cases}
\tag{10}
$$

and $d=(h-a)\cos\beta+(b-a)\sin\beta$. ε_{su} and ε_{cu} represent the ultimate steel strain and the absolute value of the ultimate compressive concrete strain, respectively. The total internal forces are computed by adding the steel and concrete contributions (see Barros *et al.* (2004) for the contribution of steel), after converting the moments furnished by expressions (4) to (8) to the central axes x_g, y_g (Fig. 4), using the expressions

$$
\begin{aligned}
M_{cx_g} &= M_{cx}\sin\beta + M_{cy}\cos\beta - N_c\frac{b}{2} \\
M_{cy_g} &= -M_{cx}\cos\beta + M_{cy}\sin\beta + N_c\frac{h}{2}
\end{aligned}
\tag{11}
$$

2.3. Extension to multi-rectangular cross sections

The stress resultants in multi-rectangular cross sections with parallel sides, as *I*, *L*, and *T* sections, may easily be computed by adding the internal forces in each rectangle. In order to develop the few supplementary expressions necessary for this task, the only new geometrical quantities needed are the coordinates x_{ci}, y_{ci}, of the nearest corner to the global reference system (x, y, Fig. 6), for each rectangle.

Given the position of the neutral axis in relation to the global reference system (x, y), defined by β and X (Fig. 6), the value of X for the computation of the stress resultants in rectangle i is given by

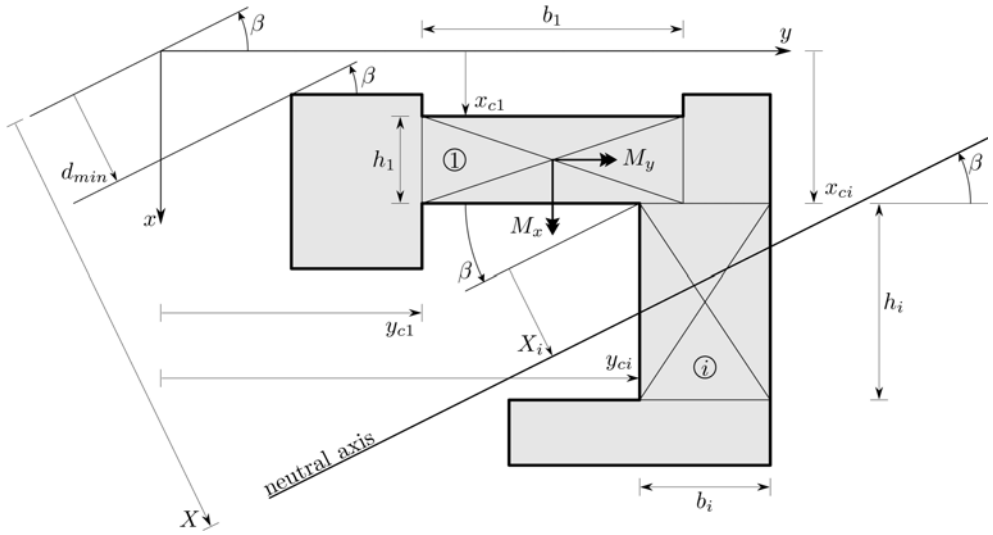

Fig. 6 Relevant geometrical data for the multi-rectangular cross section

$$X_i = X - x_{ci}\cos\beta - y_{ci}\sin\beta \tag{12}$$

The strain at the reference corner of rectangle i may be computed from the maximum compressive strain in the cross section ε_c, which occurs in the corner at the distance $d_{\min} = \min(x_{ci}\cos\beta + y_{ci}\sin\beta)$ for i=1, ..., n_r (n_r represents the total number of rectangles in the cross section), of the origin of the reference system (Fig. 6), using the expression

$$\varepsilon_{ci} = \frac{X_i}{X - d_{min}}\varepsilon_c \tag{13}$$

If the ultimate resistance of the cross section is to be computed, ε_c is given by the expressions

$$\begin{cases} \varepsilon_c = \dfrac{\alpha}{1-\alpha}\varepsilon_{su} & \text{if} \quad \alpha < \alpha_0 \\ \varepsilon_c = -\varepsilon_{cu} & \text{if} \quad \alpha \geq \alpha_0 \end{cases} \quad \text{with} \quad \alpha = \frac{X - d_{min}}{d_{tot}} \tag{14}$$

α_0 is defined in Eq. (10). The quantity d_{tot} represents the total effective height of the cross section, which is given by

$$d_{tot} = d_{max} - d_{min} \quad \text{with} \quad \begin{cases} d_{\max} = \max[(x_{ci} + h_i - a_i)\cos\beta + (y_{ci} + b_i - a_i)\sin\beta] \\ d_{\min} = \min(x_{ci}\cos\beta + y_{ci}\sin\beta) \end{cases} \tag{15}$$

for i =1, ..., n_r. a_i represents the concrete cover of rectangle i.

The internal forces in the global section are computed from the stress resultants in each of the n_r rectangles, taking the central axis of rectangle 1 (which may be any of the n_r rectangles) as reference, are given by

$$\begin{cases} N = \sum_{i=1}^{n_r} N_i \\ M_x = \sum_{i=1}^{n_r} (M_{xi} + N_i y_{gi}) \\ M_y = \sum_{i=1}^{n_r} (M_{yi} - N_i x_{gi}) \end{cases} \tag{16}$$

where N_i, M_{xi} and M_{yi} represent the stress resultants referred to the central axes of each rectangle, as given by Eq. (11), and x_{gi} and y_{gi} are the distances of the geometrical centre of each rectangle to the geometrical centre of rectangle 1.

$$\begin{cases} x_{gi} = x_{ci} + \frac{h_i}{2} - \left(x_{c1} + \frac{h_1}{2} \right) \\ y_{gi} = y_{ci} + \frac{b_i}{2} - \left(y_{c1} + \frac{b_1}{2} \right) \end{cases} \tag{17}$$

As an example of test and explanation of the used methodology, the ultimate internal forces of the rectangular cross section depicted in Fig. 7 are computed, using both the rectangular and the multi-rectangular approaches. In order to avoid gaps in the steel bands in the last approach, which would be introduced by the concrete cover, this quantity is considered zero, so that exactly the same results have to be obtained from both approaches.

The reinforcement has a constant thickness of 4 mm. In Table 1 the geometrical input data, for each of the four multi-rectangular alternatives considered, is represented.

The results obtained for a C25/30 concrete, using the Eurocode 2 (2004) constitutive law (f_{cd}=16.67 MPa, E_{cc1}=2.95, ε_{c1}=0.0022 and ε_{cu}=0.0033) and A400 steel (E=200 GPa, $f_{syd}=\frac{400}{1.15}$ MPa and ε_{su}=0.01) are presented in Table 2. Although different in what concerns the moments, as a consequence of the different reference axes (central axes of rectangle 1 in each case), these results represent exactly the same internal forces (for the number of decimal digits used in Table 2).

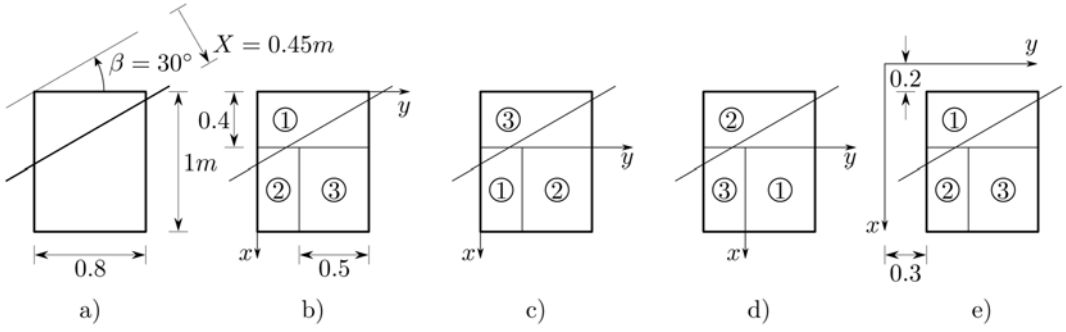

Fig. 7 Rectangular section used to test the multi-rectangle approach

Table 1 Geometrical data for the multi-rectangular cases of Fig. 7

Rectangle	b	h	x_c	y_c	a_1	a_2	a_3	a_4
1	0.8	0.4	0.0	0.0	0.004	0.004	0.004	0.0
2	0.3	0.6	0.4	0.0	0.0	0.0	0.004	0.004
3	0.5	0.6	0.4	0.3	0.004	0.0	0.0	0.004

Case b) X =0.45 m

Rectangle	*b*	*h*	x_c	y_c	a_1	a_2	a_3	a_4
1	0.3	0.6	0.0	0.0	0.0	0.0	0.004	0.004
2	0.5	0.6	0.0	0.3	0.004	0.0	0.0	0.004
3	0.8	0.4	−0.4	0.0	0.004	0.004	0.004	0.0

Case c) X=0.103589838 m

Rectangle	*b*	*h*	x_c	y_c	a_1	a_2	a_3	a_4
1	0.5	0.6	0.0	0.0	0.004	0.0	0.0	0.004
2	0.8	0.4	−0.4	−0.3	0.004	0.004	0.004	0.0
3	0.3	0.6	0.0	−0.3	0.0	0.0	0.004	0.004

Case d) X = –0.046410162 m

Rectangle	*b*	*h*	x_c	y_c	a_1	a_2	a_3	a_4
1	0.8	0.4	0.2	0.3	0.004	0.004	0.004	0.0
2	0.3	0.6	0.6	0.3	0.0	0.0	0.004	0.004
3	0.5	0.6	0.6	0.6	0.004	0.0	0.0	0.004

Case e)–X =0.773205081 m

Table 2 Ultimate internal forces in the rectangular section of Fig. 7

case	$N(N)$	$M_x(Nm)$	$M_y(Nm)$
a	−1004301.5	845134.064	−2224687.29
b	−1004301.5	845134.064	−1923396.84
c	−1004301.5	594058.689	−2425547.59
d	−1004301.5	995779.288	−2425547.59
e	−1004301.5	845134.064	−1923396.84

3. Numerical solution of the inverse problem

In the previous sections a methodology has been described which allows for the computation of internal forces (stress resultants) in the cross section, given deformation parameters: position of the neutral axis and strain in the most compressed concrete fibre. In what follows a numerical technique is presented for the solution of the inverse problem: given some or all the internal forces, computation of deformation parameters and/or the remaining internal forces or a dimensioning parameter.

The resulting non-linear system of equations is solved by means of a Newton-Raphson algorithm, with a step length limitation in order to improve robustness.

3.1. Computation of rupture envelops

The internal forces corresponding to points located on the rupture envelope defined in the N, M_x, M_y space may generally be computed by solving a system of two nonlinear equations. In fact, as the three ultimate internal forces for a given cross-section depend only on two parameters (β and X), the computation may be carried out by solving the system formed by two of the equations which define the ultimate internal forces as functions of β and X equated to given values of those forces. Taken, for example, functions M_x and M_y, we get the system of equations

$$\begin{cases} M_x(\beta,X) = \overline{M_x} \\ M_y(\beta,X) = \overline{M_y} \end{cases} \tag{18}$$

where $\overline{M_x}$ and $\overline{M_y}$ are the given internal forces. The values of β and X may be computed by means of a Newton-Raphson procedure which may be described by the algorithm

$$\underbrace{\begin{bmatrix} \frac{\partial M_x}{\partial \beta} & \frac{\partial M_x}{\partial X} \\ \frac{\partial M_y}{\partial \beta} & \frac{\partial M_y}{\partial X} \end{bmatrix}}_{\boldsymbol{A}_i} = \left(\underbrace{\begin{Bmatrix} \beta \\ X \end{Bmatrix}_{i+1}}_{\boldsymbol{x}_{i+1}} - \underbrace{\begin{Bmatrix} \beta \\ X \end{Bmatrix}_{i}}_{\boldsymbol{x}_i} \right) = \underbrace{\begin{Bmatrix} \overline{M_x} \\ \overline{M_y} \end{Bmatrix}}_{\boldsymbol{b}} - \underbrace{\begin{Bmatrix} M_x \\ M_y \end{Bmatrix}_{i}}_{\boldsymbol{b}_i} \tag{19}$$

Vector $\mathbf{b}_i$ has the values of the internal forces which correspond to the values of the geometrical parameters contained in vector $\mathbf{x}_i$. Matrix $\mathbf{A}_i$ is also computed from the values $\mathbf{x}_i$ of the unknowns. The solution of the linear system of equations represented by Eq. (19) yields the new values of the unknowns $\mathbf{x}_{i+1}$.

The derivatives contained in matrix $\mathbf{A}_i$ are numerically obtained, by considering very small increments of the unknowns β and X. For example, we have

$$\frac{\partial M_x}{\partial X} = \frac{M_x(\beta, X+dX) - M_x(\beta,X)}{dX} \tag{20}$$

where dX is a sufficiently small value to compute the derivative accurately.

With the objective of improving the robustness of the iterative procedure, by avoiding large increments in the values of the unknowns, the incremental values of β and X are limited to some given values. Taking, for example, the limits $\frac{\pi}{18}$ and $\frac{h}{10}$ for β and X, respectively, we have

$$\begin{cases} |d\beta| = |\beta_{i+1} - \beta_i| \le \dfrac{\pi}{18} \\ |dX| = |X_{i+1} - X_i| \le \dfrac{h}{10} \end{cases} \Rightarrow \begin{cases} \dfrac{18|d\beta|}{\pi} \le 1 \\ \dfrac{10|dX|}{h} \le 1 \end{cases} \tag{21}$$

The constraints defined by Eq. (21) are enforced by scaling the solution vector $d\mathbf{x}=\mathbf{x}_{i+1}-\mathbf{x}_i$ of Eq. (19) with the factor

$$\eta = \frac{1}{\psi} \quad \text{with} \quad \psi = \sqrt{\left(\frac{18 d\beta}{\pi}\right)^2 + \left(\frac{10 dX}{h}\right)^2} \tag{22}$$

if $\psi > 1$. Although, eventually, requiring more iterations, this procedure avoids convergence to undesired solutions (e.g. values of β outside the limits $0<\beta<\frac{\pi}{2}$).

Once β and X are known, the third ultimate internal force (N in this case) is directly computed using Eq. (16).

In the particular case of the computation of level curves of the rupture envelope (constant axial force N), the problem may be solved in a simpler way by fixating the value of β and computing the value of X corresponding to the given axial force N, by solving the non-linear equation.

$$N(\beta, X) = \overline{N} \tag{23}$$

This equation is also solved by means of the Newton-Raphson algorithm, that is

$$X_{i+1} = X_i + \left(\frac{\partial N}{\partial X}\right)^{-1} (\overline{N} - N_i) \tag{24}$$

A pair of values M_x, M_y is then obtained from the pair β, X by means of Eq. (16).

3.2. Dimensioning of the reinforcing steel

For a given cross-section the amount of steel needed to withstand a given set of acting internal forces N, M_x, M_y may be computed by using a similar procedure as described in the previous section. This amount is defined by the thickness of the steel bands (cf. Fig. 4). Since three equations are available and two parameters (β and X) are enough to define the ultimate internal forces, a parameter may be used to quantify the thickness of the steel bands. To this end, the following linear function is used to define that thickness

$$a_i = a_{ic} + a_{ip}\gamma \tag{25}$$

In this expression the index i denotes a steel band (i =1, .., 4) of the rectangle under consideration, a_{ic} represents a constant part of the thickness and $a_{ip}\gamma$ a part which is proportional to the dimensioning parameter γ.

The problem may be stated in the following way: given the internal forces as numerical functions of the parameters defining the position of the neutral axis, β and X, and the dimensioning parameter γ,

$$N = N(\beta, X, \gamma);\ M_x = M_x(\beta, X, \gamma) \text{ and } M_y = M_y(\beta, X, \gamma) \tag{26}$$

and prescribed values for the internal forces $\overline{N}$, $\overline{M_x}$ and $\overline{M_y}$, compute $\overline{\beta}$, $\overline{X}$ and $\overline{\gamma}$ so that we have

$$\begin{cases} N(\overline{\beta}, \overline{X}, \overline{\gamma}) = \overline{N} \\ M_x(\overline{\beta}, \overline{X}, \overline{\gamma}) = \overline{M_x} \\ M_y(\overline{\beta}, \overline{X}, \overline{\gamma}) = \overline{M_y} \end{cases} \tag{27}$$

The problem is very similar to that described in Section 3.1. The Newton-Raphson algorithm may, in this case, be described by the expression

$$\underbrace{\begin{bmatrix} \frac{\partial N}{\partial \beta} & \frac{\partial N}{\partial X} & \frac{\partial N}{\partial \gamma} \\ \frac{\partial M_x}{\partial \beta} & \frac{\partial M_x}{\partial X} & \frac{\partial M_x}{\partial \gamma} \\ \frac{\partial M_y}{\partial \beta} & \frac{\partial M_y}{\partial X} & \frac{\partial M_y}{\partial \gamma} \end{bmatrix}}_{\boldsymbol{A}_i} \left(\underbrace{\begin{Bmatrix} \overline{\beta} \\ \overline{X} \\ \overline{\gamma} \end{Bmatrix}_{i+1}}_{\boldsymbol{x}_{i+1}} - \underbrace{\begin{Bmatrix} \overline{\beta} \\ \overline{X} \\ \overline{\gamma} \end{Bmatrix}_{i}}_{\boldsymbol{x}_i} \right) = \underbrace{\begin{Bmatrix} \overline{N} \\ \overline{M_x} \\ M_y \end{Bmatrix}}_{\boldsymbol{b}} - \underbrace{\begin{Bmatrix} N \\ M_x \\ M_y \end{Bmatrix}_{i}}_{\boldsymbol{b}_i} \tag{28}$$

The derivatives in matrix $\mathbf{A}_i$ are computed as defined by Eq. (20). A limitation of the incremental values of the unknowns is also implemented. In this case Eq. (21) is substituted by

$$\begin{cases} |d\beta| = |\beta_{i+1} - \beta_i| \le \dfrac{\pi}{18} \\ |dX| = |X_{i+1} - X_i| \le \dfrac{h}{10} \\ |d\gamma| = |\gamma_{i+1} - \gamma_i| \le \dfrac{h}{1000} \end{cases} \Rightarrow \begin{cases} \dfrac{18|d\beta|}{\pi} \le 1 \\ \dfrac{10|dX|}{h} \le 1 \\ \dfrac{1000|\,d\gamma|}{h} \le 1 \end{cases} \tag{29}$$

which corresponds to the factor

$$\eta = \frac{1}{\psi} \quad \text{with} \quad \psi = \sqrt{\left(\frac{18d\beta}{\pi}\right)^2 + \left(\frac{10dX}{h}\right)^2 + \left(\frac{1000d\gamma}{h}\right)^2} \tag{30}$$

to be applied to vector $\mathbf{x}_{i+1}$ whenever $\psi > 1$.

4. Examples

As an example of application of the procedure expounded in Section 3.1 a level curve and a meridian of the rupture envelop of the cross-section depicted in Fig. 8 are computed. This is the

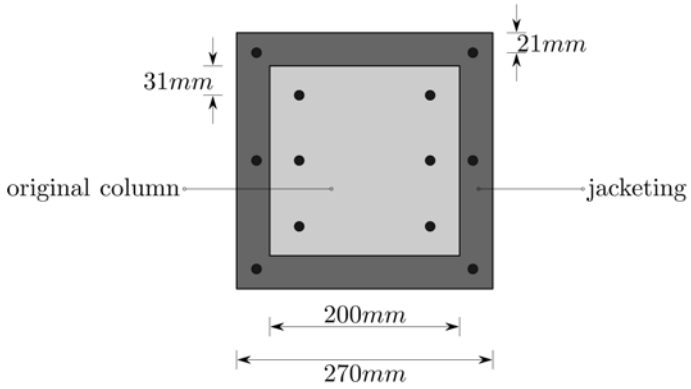

Fig. 8 Column strengthened by reinforced concrete jacketing

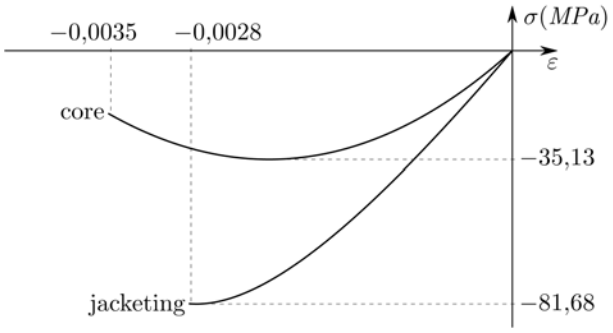

Fig. 9 Constitutive laws of the two kinds of concrete in the column of Fig. 8

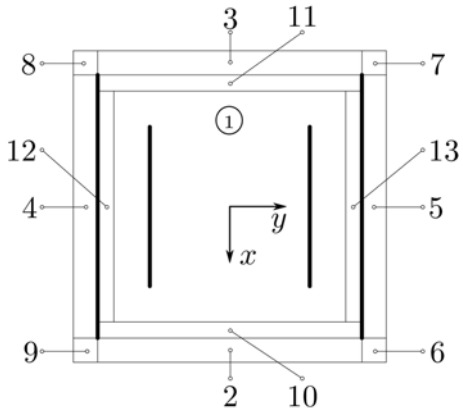

Fig. 10 Subdivision of the cross-section of Fig. 8 into 13 elementary rectangles

cross-section of a column which has been strengthened by means of reinforced concrete jacketing. Experimental data is available for the ultimate internal forces in plane bending (Júlio *et al.* 2005).

The cross-section is square and doubly symmetrical. The values indicated in the figure for the concrete cover are measured in relation to the axis of the steel bars. The diameter of the bars is 10 mm. The original (core) and strengthening concrete have the constitutive laws represented in Fig. 9, corresponding to the law defined in Eurocode 2 (2004), given the measured compressive strength. The ultimate stresses have been experimentally determined, as also the parameters dening the rheological behaviour of the steel: Young modulus E=209.456 GPa and yielding stress f_{syd}=526.102 MPa.

The cross-section has been divided into 13 rectangles, as represented in Fig. 10. The steel bands have been considered only in the faces which are parallel to axis x, since the experimental results have been obtained in plane bending around this axis. The geometrical parameters corresponding to this model (13 rectangles) are presented in Table 3.

The level curve of the rupture envelope corresponding to the compressive axial force used in the experimental test–174.7 kN–has been computed by means of the procedure defined by Eqs. (23) and (24) yielding the curve represented in Fig. 11. The experimentally obtained value in plane bending is also represented in the figure. We may observe that the error of the computed solution is smaller than 5%.

Table 3 Geometrical data corresponding to the model depicted in Fig. 10

Rectangle	b	h	a	x_c	y_c	a_1	a_2	a_3	a_4
1	0.200	0.200	0.031	-0.100	-0.100	0.001707	0	0.001707	0
2	0.228	0.021	0	0.114	-0.114	0	0	0	0
3	0.228	0.021	0	-0.135	-0.114	0	0	0	0
4	0.021	0.228	0	-0.114	-0.135	0.001033	0	0	0
5	0.021	0.228	0	-0.114	0.114	0	0	0.001033	0
6	0.021	0.021	0	0.114	0.114	0	0	0	0
7	0.021	0.021	0	-0.135	0.114	0	0	0	0
8	0.021	0.021	0	-0.135	-0.135	0	0	0	0
9	0.021	0.021	0	0.114	-0.135	0	0	0	0
10	0.228	0.014	0	0.100	-0.114	0	0	0	0
11	0.228	0.014	0	-0.114	-0.114	0	0	0	0
12	0.014	0.200	0	-0.100	-0.114	0	0	0	0
13	0.014	0.200	0	-0.100	0.100	0	0	0	0

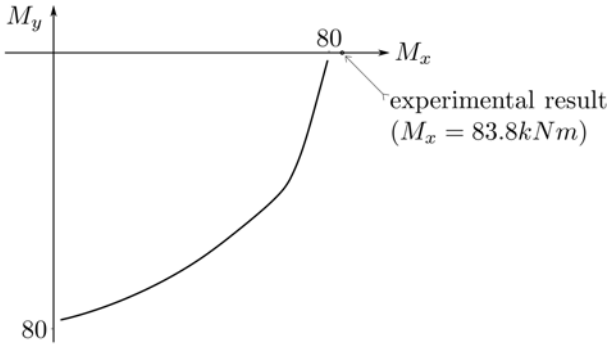

Fig. 11 Level curve of the rupture envelope for $N = -174.7$ kN

In Fig. 12 two meridians of the rupture envelope corresponding to the ratios $\frac{M_y}{M_x}$ of 0.01 and 0.05 are represented. These values, although corresponding to inclined bending are very close to the situation of plane bending which has been analysed experimentally. These curves have been computed using the algorithm represented by Eqs. (18) to (22).

As a consequence of the form of the basic equations (Eqs. (4) to (8)) it is not possible to analyse directly situations corresponding to values of β that are very close to zero or to 90° using the methodology presented in this paper, since those equations become indeterminate for β=0 or $\beta=\frac{\pi}{2}$. Thus, in the cross-section of Fig. 8 the plain bending case cannot be directly analysed. Figs. 11 and 12 show, however, that we can get sufficiently close to these values of β, so that this restriction does not have practical significance.

The experimentally obtained value for the rupture load corresponds to the highest ordinate of the load-displacement curve of a vertical cantilever column with a horizontal load applied at the top. Rupture took place by compressive concrete failure, with a strain of 1.8% in the most tensioned steel bar.

As an example of application of the algorithm described in Section 3.2 let us consider the cross-

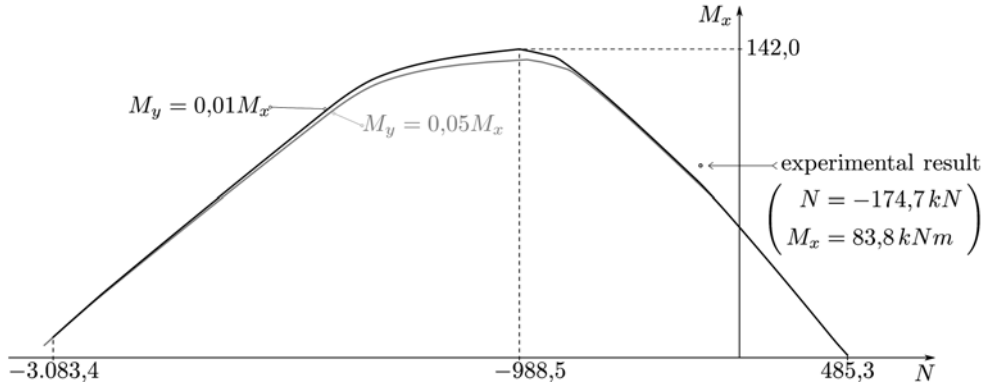

Fig. 12 Meridians of the rupture envelope for $M_y = 0.01M_x$ and $M_y = 0.05M_x$

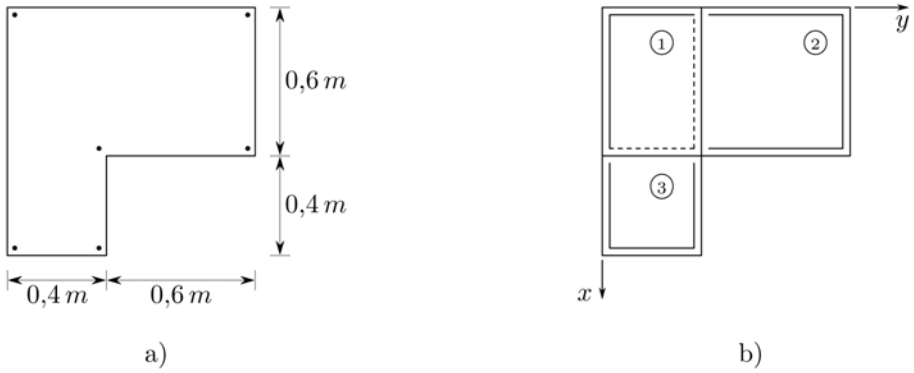

Fig. 13 Dimensioning of the reinforcement bars in a multi-rectangular cross-section

Table 4 Geometrical data corresponding to Eq. (25) for the model of Fig. 13(b)

a_c	a_p
0.37	0
0	1
0	1
0.59	0

Rectangle 1

a_c	a_p
0	1
0	1
0	0
0	1

Rectangle 2

a_c	a_p
0	1
0	0
0	1
0	1

Rectangle 3

section represented in Fig. 13(a). The member is made of concrete C25/30 and steel A400. Steel bars of diameter 16 mm with a uniform spacing shall be used.

In Fig. 13(b) the computation model is represented. The dashed lines represent the steel band corresponding to the steel bar located in the concave corner of the cross-section. The concrete cover, measured with respect to the axes of the steel bars is 3 cm. The geometrical data corresponding to Eq. (25) is represented in Table 4.

The design internal forces are N=–2000 kN, M_x =550 kNm and M_y =1200 kNm.

The bending moments are defined with respect to axes with the same directions as x and y, located at the centroid of rectangle 1. The iterative process described in Section 3.2 yielded the

Table 5 Results obtained for the model of Fig. 13(b), considering the diagrams represented in Figs. 1 and 2 for the concrete behaviour

	β (degrees)	X (m)	γ (mm)
Diagram of Fig. 1 (CEB-FIP MC90 (1991))	36.2450083	0.518968107	2.98876117
Diagram of Fig. 2 (Eurocode 2 (2004))	36.0520839	0.501651426	2.89490696

results indicated in Table 5. These results, with the degree of accuracy represented by the values indicated in Table 5, have been obtained after 6 iterations in both cases, when the starting values for the unknowns are β=45º, X=0.5 m and γ=1 mm. With the starting values: β=15º, X=0.1 m and γ =0.1 mm, which are less close to the solution, 12 iterations are needed for the same degree of accuracy. Besides, in the latter case, convergence is only achieved if the limitation of the incremental values of the unknowns described by Eqs. (29) and (30) is used.

5. Conclusions

A tool for the analysis and dimensioning of reinforced concrete prismatic members with rectangular and multi-rectangular cross-section is presented. Since the algorithm is directly based on an analytical approach, no discretization-induced errors are introduced. Besides, the algorithm is very fast showing negligible computation times, even for a large number of rectangles or for a large number of solutions, as for the case of drawing rupture envelops.

The approach has been tested for the computation of ultimate internal forces and rupture envelops and for the dimensioning of reinforcing steel. In the case of the computation of rupture envelops, experimental results are available, so that a comparison between experimental and numerical results is presented.

A procedure of step limitation has been introduced in the iterative solution of the inverse problem in order to improve the robustness of the algorithm, which has proven to be very effective.

References

Alfano, G., Marmo, F. and Rosati, L. (2007), "An unconditionally convergent algorithm for the evaluation of the ultimate limit state of rc sections subject to axial force and biaxial bending", *Int. J. Numer. Meth. Eng.*, **72**(8), 924-963.

Alfano, G., Marmo, F. and Rosati, L. (2008), "Enhanced solution strategies for the ultimate strength analysis of composite steel-concrete sections subject to axial force and biaxial bending", *Comput. Method. Appl. M.*, **197**(9-12), 1033-1055.

Bonet, J.L., Romero, M.L., Miguel, P.F. and Fernandez, M.A. (2004), "A fast stress integration algorithm for reinforced concrete sections with axial loads and biaxial bending", *Comput. Struct.*, **82**(2-3), 213-225.

Brondum, T. (1987), "Ultimate flexural capacity of cracked polygonal concrete sections with circular holes under biaxial bending", *ACI Concrete Int.*, **84**(3), 212-215.

Charalampakisa, A.E. and Koumousis, V.K. (2008), "Ultimate strength analysis of composite sections under biaxial bending and axial load", *Comput. Method. Appl. M.*, **39**(11), 923-936.

Comité Euro-internacional du beton (1991), "CEB-FIB Model Code 1990", C. E. B. Bulletin No. 203-204, y205.

De Vivo, L. and Rosati, L. (1998). "Ultimate strength analysis of reinforced concrete sections subject to axial force and biaxial bending", *Comput. Method. Appl. M.*, **166**, 261-287.

European Committee for Standardization: Eurocode 2 (2004), "Design of concrete structures-Part 1: General rules and rules for buildings", EN 1992-1-1, Brussels, December.

Fafitis, A. (2001), "Interaction surfaces of reinforced-concrete sections in biaxial bending", *J. Struct. Eng-ASCE,* **127**(7), 840-846.

Júlio, E.S., Branco, F. and Silva, V.D. (2005), "RC Jacketing interface inuence on monotonic loading response", *ACI Struct. J.,* **102**(2), 252-257.

Maple 8, *http://www.maplesoft.com*

Barros, M.H.F.M., Barros, A.F.M. and Ferreira, C.C. (2004), "Closed form solution of optimal design of rectangular reinforced concrete sections", *Eng. Computation*, **21**(7), 761-776.

Barros, M.H.F.M., Ferreira, C.C. and Barros, A.F.M. (2005), "Closed form interaction surfaces for nonlinear design codes of reinforced concrete columns with model code 90", *Comput. Concrete,* **2**(1), 55-77.

Rodriguez, J.A. and Aristizabal-Ochoa, J.D. (1999), "Biaxial Interaction Diagrams for Short RC Columns of Any Cross Section", *J. Struct. Eng-ASCE,* **125**(6), 672-683.

Sfakianakis, M.G. (2002), "Biaxial bending with axial force of reinforced, composite and repaired concrete sections of arbitrary shape by fiber model and computer graphics", *Adv. Eng. Softw.*, **33**(4), 227-242.

Yen, J.R. (1991), "Quasi-Newton method for reinforced concrete column analysis and design", *J. Struct. Eng-ASCE,* **117**(3), 657-666.

Zupan, D. and Saje, M. (2005) "Analytical integration of stress field and tangent material moduli over concrete cross-sections", *Comput. Struct.* **83**(28-30), 2368-2380.

CC